Materials Science-Poland, *Vol. 28*, *No. 2*, *2010*

Structural, morphological and electrochemical characterization of electron beam deposited $Li_{1+x}Mn_2O_4$ (x = 0, 0.05) thin films

S. BALAJI[1*], S. SHANMUGAN[1], D. MUTHARASU[2], K. RAMANATHAN[1]

[1]Materials Laboratory, Thiagarajar Advanced Research Centre,
Thiagarajar College of Engineering, Madurai-625 015, Tamil Nadu, India

[2]School of Physics, University Sains Malaysia, 11800, Penang, Malaysia

$Li_{1+x}Mn_2O_4$ (x = 0, 0.05) powders were synthesized using the microwave assisted co-precipitation method. Materials were evaporated using an electron beam gun. Structural analyses of thin films coated over platinum substrates revealed their cubic structure. The lattice constant of $Li_{1.05}Mn_2O_4$ thin film was found to be around 8.2475 Å. The lattice constant of $Li_{1.05}Mn_2O_4$ Powder was found to be 8.2488 Å. Morphological properties of the coated films were studied by SEM and the obtained micrographs were analyzed using the Image-j software. The roughness and the porosity were observed to be higher for the samples containing an excess of Li. The thin films were subjected to electrochemical characterization in aqueous $LiNO_3$ solution; cyclic voltammograms obtained for the samples revealed two sets of well defined redox peaks around 0.07 and 0.1 V in $LiNO_3$ solution. The redox peaks in $Li_{1.05}Mn_2O_4$ thin film samples had lower intensities than those of the stochiometric compound.

Keywords: *$LiMn_2O_4$; microwave synthesis; electron beam evaporation*

1. Introduction

Miniaturization of electronic devices has resulted in very low current and power requirements for many applications. Microenergy sources such as thin film battery devices have been developed to power these microelectronic devices. Lithium manganese oxide has been studied as a promising cathode material for lithium ion batteries, owing to its low cost, ease of preparation, and environmental harmlessness when compared with conventional $LiCoO_2$ [1]. In order to obtain efficient performance, thin film electrodes are expected to possess correct stoichiometry, good crystallinity and excellent adherence to the substrate. Much effort has been made for the fabrication of

*Corresponding author, e-mail: sbalaji@tce.edu

thin film electrodes using various deposition techniques such as electron beam evaporation, RF magnetron sputtering, pulsed laser deposition, chemical vapour deposition, etc. [2–4]. Even though the RF sputtering method has attracted a great deal of attention, due to the reproducibility of thin films that have good adherence, it requires high vacuum conditions, inert gases and high purity or high density targets. As a result, electron beam deposition has emerged as an alternative to RF sputtering, since it does not require highly voluminous electrode materials and sophisticated vacuum equipment. Moreover, the main advantage of this method is that doping cations can be added during deposition, which occludes the capacity fading of $LiMn_2O_4$ [5].

The conventional solid state reaction of mixing oxides or carbonates is widely adopted for the synthesis of $LiMn_2O_4$. Since the method has various limitations like high temperature processing, longer processing time, chemical inhomogeneity of the product and coarser particle size, several methods have been developed by many authors to obtain phase pure and smaller grain size products. Recently, a novel method, known as the microwave synthesis method, has been developed to prepare cathode materials for lithium ion batteries [6, 7]. In the microwave irradiation field, since the microwave energy is absorbed directly by the heated object, uniform and rapid heating can be achieved within several minutes. Such rapid synthesis may deliver fine powder, due to the suppressed diffusion process of growing crystal particles.

Conventionally, the electrochemical performances of the cathode materials are studied in the non-aqueous electrolytes, owing to their stability in the electrolyte and their reversibility during cycling. But the development of alternative Li ion cells has paved the way to identify new electrolytes including aqueous electrolytes. Recently Dahn et al. reported the charge and discharge properties of $LiMn_2O_4$ in aqueous solutions of LiOH and $LiNO_3$ [8], showing that aqueous electrolytes can be used to replace non-aqueous ones for the preliminary study of cathode materials for lithium battery applications.

In the present paper, the microwave synthesis of $Li_{1+x}Mn_2O_4$ (x = 0, 0.05) has been presented as well as evaporation of materials through an electron beam gun on a polycrystalline platinum substrate and the relevant structural properties.

2. Experimental

$LiMn_2O_4$ (sample A) and $Li_{1.05}Mn_2O_4$ (sample B) have been fabricated by the microwave assisted co-precipitation method. Manganese acetate was dissolved with desired stochiometric quantity in double distilled water and the solution has been pumped into reaction vessel with continuous stirring. At the same time, 2 M NaOH aqueous solution has been separately fed into the reaction vessel. The pH of the solution has been maintained at 10.0, stirring speed has been fixed at 60 r.p.m. and the temperature has been controlled at 60 °C. The precipitated $Mn(OH)_2$ was filtered and washed. The obtained powders were dried at 110 °C to remove adsorbed water and mixed thoroughly with $LiOH{\cdot}H_2O$ powder of required quantity.

The grounded powder was calcined in a microwave furnace in two steps. Initially, small pellets of 1 cm in diameter were heated to 500 °C for 10 min, and then calcined at 800 °C for about 20 min. In practice, many materials could not couple with microwave directly in the room temperature and hence it would be necessary to preheat them. Since the dielectric loss of the material increases with temperature, low dielectric loss materials could be made absorptive by raising their temperature [9]. Most commonly, the specimen would be enshrouded by room temperature susceptor material to supply thermal energy by heat transfer and hence the specimen would be subjected simultaneously to thermal and electromagnetic energy. In this case, SiC granules have been used as susceptors which could readily combine with microwave and boost the temperature so as to enable the sample to couple directly with the field [10]. The samples were digested in concentrated HCl and subjected to ICP-AES compositional analyses.

The electron beam evaporation of the samples synthesized via the microwave synthesis was carried out under the vacuum range of 7×0^{-6} mBar, the potential applied between the electrodes was kept constant at 6 kV, the emission current was maintained at 50 mA and the distance between the source and substrate was 7 cm. In order to achieve uniform and homogeneous deposition, the substrate holder rotation was carried out at 40 r.p.m. using a rotary drive. The films were coated over polycrystalline platinum substrate and the thicknesses of the films have been maintained around 4 μ and controlled during the deposition using an in-built quartz crystal monitor. After annealing at 600 °C in the ambient atmosphere, the coated films were subjected to structural and electrochemical characterization.

The structural characterization of the samples was carried by the X-Ray powder diffraction method, using a Philips PW 1710 diffractometer with automatic data acquisition. All scans were recorded for 2θ ranging from 10° to 80°. The indexation was carried out based on the JCPDS standards. The lattice parameters were calculated using the 'Powder-X' software. The scanning electron microscopy was performed using JEOL, JSM-6460 equipment. Three representative areas were randomly selected and scanned in vertical direction and a series of sequential images was recorded for each selected area. The micrographs were subjected to image processing using the Image-J software.

The electrochemical characterizations have been performed using Micro auto lab with FRA III model potentiostat/galvanostat equipment. The Ag/AgCl with 3M KCl (E = 0.208 V versus SHE) and platinum was used as a reference electrode and a counter electrode, respectively. Thin film electrodes on platinum substrate were used as working electrodes and 9 M aqueous solution of $LiNO_3$ was used as the electrolyte. The electrodes were stable throughout the experimentation in the electrolyte. Initially the lithiated electrodes were believed to react with water in aqueous solutions but the work of Dahn et al. has proved their stability [11]. Upon increasing concentration of Li^+ ions in the electrolyte, the chemical potential of the Li^+ ions would also increase; thereby the reaction with water could be eliminated. The detailed reaction has been

presented in Sect. 3.3. The cyclic voltammetry of the samples was recorded after de-aerating the cell with N_2 for more than 10 min.

3. Results and discussion

3.1. Structural characterization

Figure 1 shows the X-ray diffraction pattern of powder sample A calcined in a microwave furnace at 800 °C for 20 min and the respective thin film, evaporated using electron beam gun. The observed diffraction patterns for both powder and thin film samples could be indexed to a cubic unit cell with *Fd*3*m* space group and good agreement has been obtained with the JCPDS standard (file No. 35-0782) for $LiMn_2O_4$ powder.

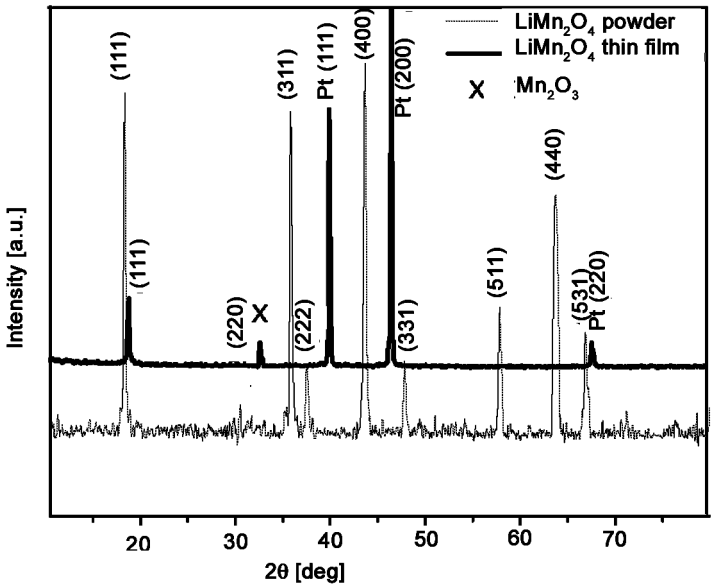

Fig. 1. XRD patterns of $LiMn_2O_4$ powder sintered at 800 °C in a microwave furnace and of $LiMn_2O_4$ thin film annealed at 600 °C

The lattice parameter of sample A was around 8.248 Å, which is comparable with the lattice parameter as per the JCPDS standard around 8.2476 Å. For the powder samples, the peaks corresponding to 2θ – 18.35, 35.814, 43.6, 57.85 and 63.546 were assigned to the planes (111), (311), (400), (511) and (440), respectively. The existence of the above peaks confirms the formation of the spinel phase of $LiMn_2O_4$; lithium ions occupy there tetrahedral sites (8a), Mn^{3+}, Mn^{4+} ions occupy octahedral sites and O^{2-} ions are located at 32e sites [12]. In general, the impurity peaks corresponding to MnO_2 and Mn_2O_3 have usually been observed in microwave synthesis by many au-

thors due to the lithium loss during evaporation and thereby lead to formation of compounds with lower concentrations of lithium. But the observed result for powder samples reveals the formation of single phase $LiMn_2O_4$ without any impurity phases, if microwave heating is set at 800 °C for 20 min. This may be due to the rapidity of microwave processing, resulting in a thermodynamically more favourable structure in a much shorter time, and thereby possible phase transitions might be avoided. The results were cross-checked with the ICP-AES measurements. ICP-AES analyses showed the Li/Mn molar ratios for the powder specimens of sample A and sample B were around 1.013/1.9877 and 1.0506/2.0062, respectively.

The XRD pattern corresponding to a thin film of $LiMn_2O_4$ material is shown in the same figure. It was observed to possess a preferred orientation of (111). However, the lattice parameters of the powder (8.2488 Å) and thin film (8.1305 Å) samples exhibit a marked difference. A small impurity peak corresponding to Mn_2O_3 is visible in the thin film sample, and this may be due to the lithium loss during the evaporation. Hence the compensation of the Li loss during evaporation has been observed to be necessary. Quantitative analyses of thin films by ICP-AES testing further clarify the above observation. Thin films, after being dissolved in concentrated HCl were subjected to ICP-AES analysis. The Li/Mn ratio in thin film of sample A was observed to be around 0.63/2.23.

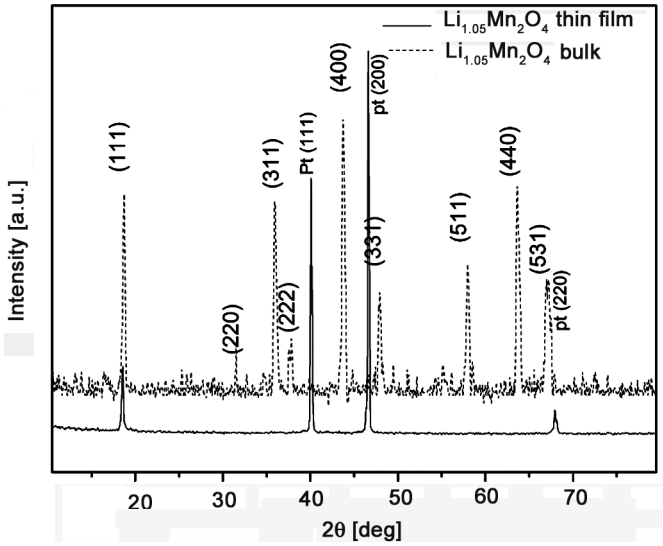

Fig. 2. XRD patterns of $Li_{1.05}Mn_2O_4$ powder sintered at 800 °C in microwave furnace and of $Li_{1.05}Mn_2O_4$ thin film annealed at 600 °C

To compensate for Li loss, a sample with 5% lithium excess was fabricated. The XRD patterns of the powder and thin film of such samples are shown in Fig. 2. The powder sample showed very good conformity with the JCPDS standard (file No. 35-0782). The lattice constant, however, has been found to be much higher than that of

$LiMn_2O_4$. This observation is in close agreement with the report made by Ohzuku et al. on changes in the lattice constant in spinel-related manganese dioxide $Li_xMn_2O_4$ ($0 \le x \le 2$) [13]. Due to the increase in the lithium concentration, the unit cell volume expansion may occur, which is evident from the increase in the lattice parameter for $Li_{1.05}Mn_2O_4$. However the formation of impure phases has been occluded during the evaporation of materials into thin films and this is evident from the diffraction pattern of the $Li_{1+x}Mn_2O_4$ thin film sample. The diffraction pattern of the thin film sample corresponded to a single $LiMn_2O_4$ phase with a preferred orientation in the [111] plane. Furthermore, differences between the lattice constants of $LiMn_2O_4$ powder (8.2488 Å), $Li_{1+x}Mn_2O_4$ powder (8.2533Å) and $Li_{1+x}Mn_2O_4$ thin film sample (8.2475Å) were observed to be negligible. Moreover, the unit cell dimensions of the $Li_{1+x}Mn_2O_4$ thin film sample and the $LiMn_2O_4$ bulk sample are very similar . Hence it is logical to conclude that the addition of extra lithium in the compound compensates for the lithium loss which occurs during thin film vapour deposition. The above conclusion is confirmed by ICP-AES analysis of the thin film sample. Quantitative analysis of thin film of sample B showed the Li/Mn ratio to be around 0.932/2.045.

The structural parameters are shown in Table 1.

Table 1. Structural parameters of powders and thin films

Sample	FWHM	Lattice constant [Å]	Crystallite size [nm]	Strain [$lines^{-2\cdot0}\cdot m^{-4}$]	Dislocation density [$\times10^{-18}$ $lines\cdot m^{-2}$]
$LiMn_2O_4$ (powder)	0.2606	8.248	32.2	0.0643	0.00096
$Li_{1.05}Mn_2O_4$ (powder)	0.2997	8.253	28.0	0.0739	0.00127
$LiMn_2O_4$ (thin film)	0.2717	8.131	30.9	0.0669	0.00104
$Li_{1.05}Mn_2O_4$ (thin film)	0.2647	8.247	31.6	0.0670	0.00100

The strain and dislocation density of the films were calculated using the equations [14]

$$\text{strain}(\varepsilon) = \frac{\beta \cos\theta}{4} \tag{1}$$

$$\text{dislocation density} = \frac{1}{D^2} \tag{2}$$

where D denotes the crystallite size, and β is the full width at half maximum. In general, in any compound, the internal strain and dislocation that cause defects are typically attributable to various processes involved during the formation of the compound. Moreover, according Chung et. al., the electrochemical performance of the $LiMn_2O_4$

electrode for cycling at 4 V region depends on the Li content being directly proportional to the strain in the crystal lattice [15]. Hence, if we could reliably measure the internal strain and the dislocation density, we would gain better understanding about the formation of compounds. The strain and dislocation density have been identified as the key parameters determining the quality of the films, thus their measurement is of fundamental importance. Since the dislocation density and strain are the manifestation of dislocation networks in the films, the decrease in the strain and dislocation density, when compared with the non-stochiometric powder sample B, indicates the formation of higher quality films at higher annealing temperatures.

The lattice strain increases with the Li concentration in the powder sample, and which is obvious because of the lattice expansion (Table 1). The strain of $Li_{1.05}Mn_2O_4$ thin film is comparable to that of $LiMn_2O_4$ powder, which shows the compensation of lithium loss by stoichiometric excess of Li. The crystallite sizes of the samples have been calculated using the Debye–Scherrer formula. The crystallite sizes for both the powder and the thin film samples were observed to be of the order of 30 nm.

3.2. Morphological studies

The scanning electron micrographs showing the morphological features of the $Li_{1+x}Mn_2O_4$ (x = 0, 0.05) thin films are shown in Fig 3. The micrographs were subjected to image processing using 'Image-J' software [16].

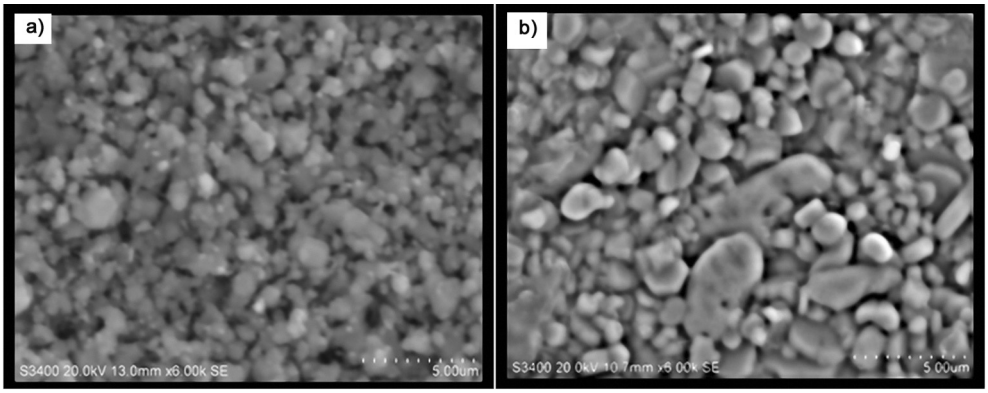

Fig. 3. Scanning electron micrograph of thin film samples of: a) $LiMn_2O_4$, b) $Li_{1.05}Mn_2O_4$

The image processing was carried out in four stages, namely de-noising, pore shape regularization, binarisation and quantification of relevant features to ascertain porosity, pore size distribution and surface texture. The de-noising has been carried out using a median filter and the pore shape regularization and binarisation were carried out using 'BinariseSEM' Java plug-in provided in the software. The porosity, pore area, pore aspect ratio and grain size were determined by the 'ComputeStats' Java plug-in provided in the software. The surface texture and roughness were com-

puted using the '3D' and 'Roughness calculation' Java plug-ins. The 3D surface texture and the pore area distribution are shown in Fig. 4, and in Table 2, the morphological parameters are given.

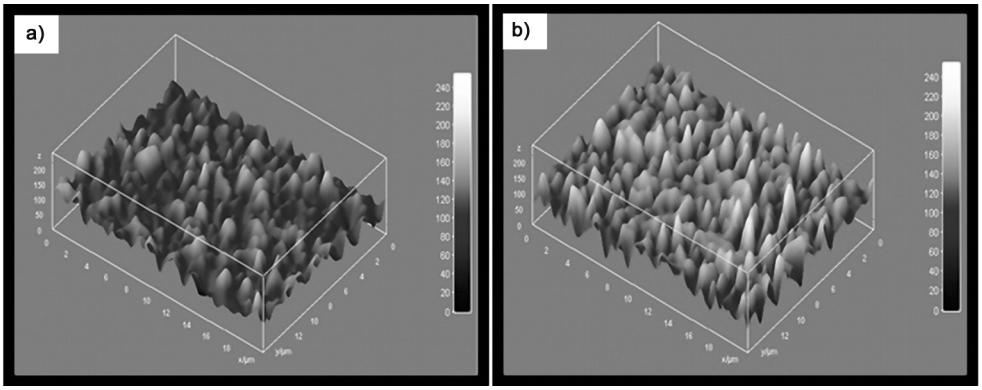

Fig. 4. 3D surface plot of thin film samples: a) $LiMn_2O_4$, b) $Li_{1.05}Mn_2O_4$

Table 2. Morphological parameters of thin films

Sample	Mean grain size [μm]	Pore area $[\mu m]^2$	Pore aspect ratio	Porosity	Pore size [μm]	Roughness [nm]	
						RMS	AM
$LiMn_2O_4$	0.708	23.207	1.632	0.377	20.455	106.654	102.324
$Li_{1.05}Mn_2O_4$	0.485	61.272	1.809	0.593	25.186	128.562	127.244

The porosity is considered to be one of the major properties influencing the electrochemical properties. For higher porosity, the electrochemically active surface area is greater, (i.e., the area of contact between the electrode and the electrolyte is greater). Hence, in order to obtain efficient electrode performance, high surface area electrodes are generally preferred. In the samples, the reduction in grain size, increase of the porosity and pore aspect ratio of thin films with increasing lithium concentration has been observed (Table 2). The observed increase in the pore aspect ratio may be considered an encouraging effect because upon increasing the pore aspect ratio, the contact area between the electrolyte and the cathode also increases, thereby improved electrochemical performance can be achieved. The root mean square roughness has also been observed to increase as Li concentration in thin films increases, and this is consistent with the effect observed by Siemen et al. [17].

3.3. Electrochemical studies

Figure 5 shows typical second cycle cyclic voltammograms of thin film electrodes $Li_{1+x}Mn_2O_4$ (x = 0, 0.05) in a solution of 9 M $LiNO_3$ under quasi-steady state condition

with low potential scan rate (0.5 mV/s). Generally for lower scan rates, the peak current would be high because electrolysis will be completed after long time [18]. On the other hand, this behaviour may also be due to the fact that the electrode is thin enough so that at the scan rate employed, the diffusion layer reaches the film edge, which is called 'finite diffusion', and causes complete oxidation or reduction. For higher scan rates, the peak current has been observed to decrease and hence it is not included in this investigation.

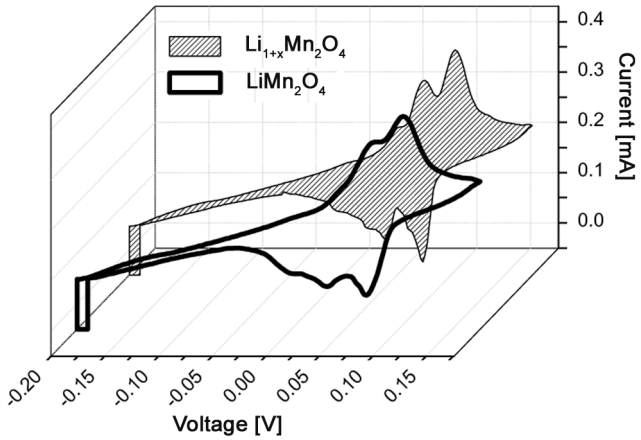

Fig. 5. Cyclic voltammogram of $Li_{1+x}Mn_2O_4$ (x = 0, 0.05) thin film in 9 M $LiNO_3$ aqueous solution

The cyclic voltammograms obtained for $LiMn_2O_4$ shown in Fig. 5 reveal two sets of well defined redox peaks in $LiNO_3$ solution being in good agreement with those obtained for the electrodes in non-aqueous solutions [19]. This indicates that intercalation of Li ions is also feasible in aqueous solutions. These four peaks are considered to be indications of the order–disorder phase transitions of $LiMn_2O_4$ due to the interactions between the electrode and Li^+ ions in the electrolyte. The presence of two peaks during discharging may be attributed to phase transitions during the insertion of Li ions in aqueous solutions [20].

The charge–discharge mechanism of $Li_xMn_2O_4$, in aqueous solution may be described as follows:

$$Li_xMn_2O_4 + \Delta x Li^+ + \Delta x e^- \underset{\text{discharging}}{\overset{\text{charging}}{\longleftrightarrow}} Li_{x+\Delta x}Mn_2O_4 \tag{3}$$

If the amount of intercalating Li ions increases, the formation of tetragonal phases should also emerge but no such redox peak corresponding to tetragonal phases have been observed. The formation of tetragonal phases is mainly because of the Jahn–Teller distortion which is an irreversible phase transition and results in diminishing of the capacity of the electrode. The absence of the lower voltage peak in the second cycle illustrates the stability of the oxide cathode in the voltage window under investigation.

In general, during intercalation of lithium ions from aqueous solutions, unwanted oxidation and reduction of water species may occur according to equation below results in a change in the pH of the electrolyte solution [21]:

$$Li_x(Host) + xH_2O \leftrightarrow Host + xLiOH(aq) + x/2H_2(g) \quad (4)$$

Hence, in order to reduce the effect of oxidation or reduction of water, the electrolyte having a higher concentration of lithium was chosen so that the chemical potential of Li^+ ions in the solution increases as the concentration of Li^+ ions in the electrolyte increases. Hence, the forward reaction of the above equation becomes less favourable. This was confirmed by constant value of pH during the experiment. The peak split in Fig. 5 was more pronounced for thin film of sample B. This shows that the formation of lithium manganese oxide has been improved in the film and the absence of extra redox couple responsible for tetragonal phase inset due to extra lithium in tetrahedral sites could be attributed to the compensation of lithium loss.

4. Conclusions

$Li_{1+x}Mn_2O_4$ (x = 0, 0.05) powders were successfully prepared by microwave processing. XRD patterns of the powder samples $Li_{1+x}Mn_2O_4$ (x = 0, 0.05), reveal the presence of a single phase compound having no impurity phases, showing that microwave processing is not associated with athermal effects and introducing impurities. XRD patterns for thin film samples reveal the formation of a compound with single phase. It is also observed that the evaporation of the $Li_{1.05}Mn_2O_4$ sample has yielded predominant (111) orientation with lesser strain. The cyclic voltammetry results, with two strong sets of red-ox peaks, also indicate the feasibility of intercalation of Li ions in aqueous solutions. The intercalation behaviour is observed to improve with increase in lithium content in the powder sample. Hence it is expected that excessive Li^+ doping can compensate for the lithium loss which occurs during evaporation of the cathode materials. It is also expected that microwave processing may be used to synthesize cathode materials for Li ion batteries in a shorter time and with good stoichiometric control.

Acknowledgements

The authors express their gratitude to the Principal and Management of Thiagarajar College of Engineering, Madurai, for their support as well as the Research Centre Imarat, India for their financial support. The SAIF-STIC, Cochin University is acknowledged for ICP-AES measurements.

References

[1] GADJOV H., GOROVA M., KOTZEVA V., AVDEEV G., UZUNOVA S., KOVACHEVA D., J. Power Sources, 134 (2004), 110.

[2] BATES J.B., DUDNEY N.J., GRUZALSKI G.R., ZUHR R.A., CHOUDHURY A., LUCK C.F., J. Power Sources, 43–44 (1993), 103.

[3] ROUGIER A., STRIEBEL K.A., WEN S.J., CAIRNS E.J., J. Electrochem. Soc., 145 (1998), 2975.
[4] FRAGNAUD P., NAGARAJAN R., SCHLEICH D.M., VUJIC D., J. Power Sources, 54 (1995), 362.
[5] SHOKOOHI F.K., TARASCON J.M., WIKENS B.J., GUYOMARD D., CHANG C.C., J. Electrochem. Soc., 139 (1992), 1845.
[6] HARISH BHAT M., CHAKRAVARTHY P., RAMAKRISHNAN A., LEVASSEUR., RAO K.J., Bull. Mater. Sci., 23 (2000), 461.
[7] YEN PEI FU., YU HSIU SU., CHENG HSIUNG LIN., SHE HUANG WU., J. Mater. Sci., 41 (2006), 1157.
[8] ALI EFTEKHARI., Electrochim. Acta, 47 (2001), 495.
[9] SPOTZ S., SKAMSER D.J., JOHNSON D.L., J. Am. Ceram. Soc., 78 (1995), 1041.
[10] RAMESH P.D., BRANDON D., SCHACHTER L., Mat. Sci. Eng., A266 (1999), 211.
[11] LI W., DAHN J.R., WAINWRIGHT D.S., Science, 264 (1994), 1115.
[12] ARORA P., POPOV B.N., WHITE R.E., J. Electrochem Soc., 145 (1998), 807.
[13] OHZUKU T., KITAGAWA M., HIRAI T., J. Electrochem. Soc., 137 (1990), 769.
[14] LALITHA S., SATHYAMOORTHY R., SENTHILARASU S., SUBBARAYAN A., NATARAJAN K., Sol. En. Mater. Sol. Cells, 82 (2004), 187.
[15] CHUNG K.Y., KIM K.B., Electrochim. Acta, 49 (2004), 3327.
[16] Research Services Branch NIMH & NINDS Image J., Image processing and analysis in Java Available via Web site: http://rsb.info.nih.gov/ij.
[17] SIMMEN F., LIPPERT T., NOVÁK P., NEUENSCHWANDER B., DÖBELI M., MALLEPELL M., WOKAUN A., Appl. Phys. A, 93 (2008), 711.
[18] LI W., MCKINNON W.R., DAHN J.R., J. Electrochem. Soc., 141 (1994), 2310.
[19] GUMMOW R.J., DE KOCK A., THACKERAY M.M., Solid State Ionics, 69 (1994), 59.
[20] WANG PEI, YANG HU, YANG HUAQUAN, J. Power Sources, 63 (1996), 275.
[21] JAYALAKSHMI M., MOHAN RAO M., SCHOLZ F., Langmuir, 19 (2003), 8403.

Received 9 May 2009
Revised 20 October 2009